

Magnetically induced chessboard pattern in the conductance of a Kondo quantum dot

M. Stopa¹ and W.G. van der Wiel²

¹ERATO-JST, 4S-308S, NTT Atsugi Research and Development Laboratories,
3-1 Morinosato-Wakamiya, Atsugi-shi Kanagawa-ken, 243-0198 Japan

²PRESTO-JST; University of Tokyo, 7-3-1, Hongo, Bunkyo-ku, Tokyo 113-0033, Japan; Department of NanoScience and DIMES, Delft University of Technology, PO Box 5046, 2600 GA Delft, The Netherlands

S. De Franceschi³, S. Tarucha⁴ and L.P. Kouwenhoven³

³ERATO-JST, Department of NanoScience and DIMES, Delft University of Technology,
PO Box 5046, 2600 GA Delft, The Netherlands

⁴ERATO-JST, University of Tokyo, 7-3-1, Hongo, Bunkyo-ku, Tokyo 113-0033, Japan

We quantitatively describe the main features of the magnetically induced conductance modulation of a Kondo quantum dot – or chessboard pattern – in terms of a constant-interaction double quantum dot model. We show that the analogy with a double dot holds down to remarkably low magnetic fields. The analysis is extended by full 3D spin density functional calculations. Introducing an effective Kondo coupling parameter, the chessboard pattern is self-consistently computed as a function of magnetic field and electron number, which enables us to quantitatively explain our experimental data.

A quantum dot [1] with a finite net electron spin strongly coupled to its leads, enabling higher-order cotunneling processes, is able to exhibit the Kondo effect [2,3]. The Kondo effect in quantum dots manifests itself as an enhanced conductance in the Coulomb blockade regime and occurs for temperatures and source-drain voltages below an energy scale set by the Kondo temperature. The first experimental results on the Kondo effect in quantum dots [4–6] were described with help of the spin-1/2 Anderson impurity model. Assuming continuous filling of spin-degenerate single-particle levels, the dot is expected to either have total electron spin $S = 0$ (for electron number N is even) or $S = 1/2$ (for N is odd). The Kondo effect is therefore only expected for odd N , hence giving rise to an “even-odd-effect” in the Coulomb valley conductance. A wide range of experiments, however, has shown a clear deviation from this picture [7–16]. Particularly striking is the observation of a “chessboard pattern” in the dot conductance as a function of magnetic field, B , and gate voltage, V_g [11,12,14–16]. Characteristic for this pattern is the alternation of high and low valley conductance regions as a function of B within the same Coulomb valley, i.e. for *constant* N . In addition, the conductance also alternates when N is changed by sweeping V_g at constant B . The distinct regions in the V_g, B plane of either high or low conductance are associated with the fields of a chessboard due to the similar appearance when the conductance is plotted in color scale (see Fig. 1b). It has been experimentally shown that the enhanced conductance in certain Coulomb blockade regions can be ascribed to the Kondo effect, for both N odd *and* even [11,12,14–16].

In this paper, we start by presenting our experimental data on a single lateral quantum dot clearly exhibiting the chessboard pattern. Next, we calculate the skeleton of the chessboard pattern with a constant inter-

action (CI) model of two capacitively interacting dots, formed by the two lowest Landau levels (LLs) – an analogy (partly qualitatively) applied before at high magnetic fields [12,18–20] – and obtain the characteristic hexago-

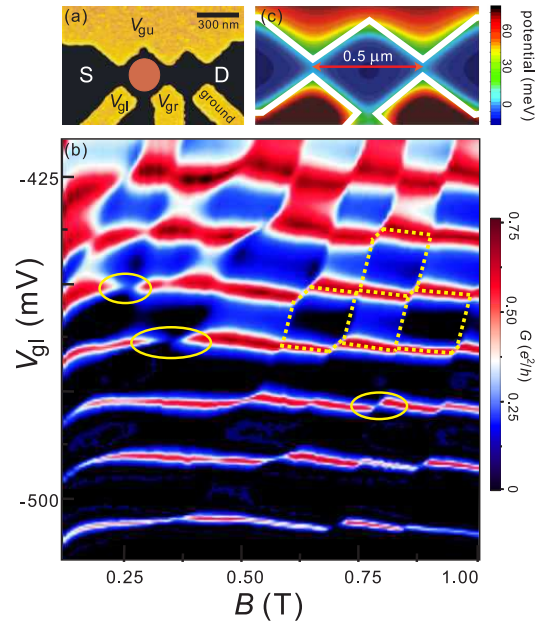


FIG. 1. (a) Scanning electron micrograph of the device. The metal gates are yellow and the dot is indicated by a red circle. The ungated 2DEG has a mobility of 2.3×10^6 $\text{cm}^2/(\text{Vs})$ and an electron density of $1.9 \times 10^{15} \text{ m}^{-2}$ at 4.2 K. The nominal dot size is $320 \times 320 \text{ nm}^2$. (b) Color scale plot of the experimental linear conductance G through the dot as a function of B and V_{gl} at 10 mK. The dotted hexagons highlight the shape of a few chessboard fields. The ellipses indicate some regions where suppression of the Coulomb peak occurs. (c) Calculated self-consistent potential landscape of the device. The white lines denote the contours of the metal gates.

nal, double dot (DD) stability diagram [17]. Interestingly, in this work we find that, due to small N and the shallow potential, higher LLs only start to fill below a *few tenths of a tesla*. Thus the DD analogy applies down to remarkably low magnetic fields. We finally perform full, 3D spin density functional (SDF) calculations for our device and introduce an effective Kondo coupling, derived entirely from the self-consistent results. Hence we can simultaneously calculate the electronic states of the dot and an estimate of the Kondo coupling, exhibiting the chessboard structure, and quantitatively explain some of its subtler features.

Our quantum dot is shown in Fig. 1a. Metal gates are deposited on top of a GaAs/AlGaAs heterostructure with a two-dimensional electron gas (2DEG) 100 nm below the surface [17]. By depleting the 2DEG below the gates, the quantum dot is defined. Current can flow from the source (S) to the drain (D) contact. The electron number is varied by sweeping the left gate voltage, V_{gl} . The SDF calculations show that our dot typically contains $\sim 20 - 40$ electrons.

Figure 1b shows a color scale plot of the linear conductance G through the dot as a function of B and V_{gl} . Red (blue) corresponds to large (small) G (see scale in Fig. 1b). For the most negative values of V_{gl} the coupling of the dot to the leads is weak. This results in relatively sharp Coulomb peaks (red lines) and low valley conductance (dark blue regions). However, if V_{gl} is increased, the valley conductance reaches considerable values ($\sim e^2/h$) in certain regions of the (B, V_{gl}) plane. Most strikingly, the regions of low and high valley conductance alternate both along the V_{gl} and the B axis in a regular fashion, resulting in the aforementioned chessboard pattern. The V_{gl} period (~ 10 mV) is set by the energy required for adding an extra electron to the dot (addition energy), whereas the B period (~ 0.1 T) corresponds to adding a flux quantum to the effective dot area. Based on the temperature dependence of G in the high valley conductance regions (not shown here), we can ascribe the enhancement of G to the Kondo effect. The transition from low to high valley conductance is associated with an abrupt jump of the V_{gl} position of the Coulomb peaks. In some cases (see ellipses in Fig. 1b) the jump is accompanied by a suppression of the peak height. Below we present a quantitative description for the experimental features discussed above, using first an intuitive, though quantitative, approach followed by a fully self-consistent simulation of our device.

In the region where the two lowest LLs, labeled LL0 and LL1, are occupied, the outline of the chessboard pattern can be considered to be a DD (Fig. 2a) stability diagram, where now B acts as one of the gates. B couples to both “dots” (i.e. LLs) but with different “lever arms.” Similarly, V_{gl} couples with different capacitances to the two LLs. We write an elementary CI functional for the

total energy, E ,

$$E(N_0, N_1) = \sum_{nm} \sum_{\sigma} \varepsilon_{nm} + \frac{1}{2D} [C_{11}(N_0e - C_{g0}V_{gl})^2 + C_{00}(N_1e - C_{g1}V_{gl})^2] - \frac{C_{01}}{D} (N_0e - C_{g0}V_{gl})(N_1e - C_{g1}V_{gl}), \quad (1)$$

where $N_{0(1)}$ is the number of electrons in LL0(1), $\varepsilon_{nm} \equiv (2n + |m| + 1)\hbar\tilde{\omega} + m\hbar\omega_c$ are the Fock-Darwin (FD) energy levels [21], and the sum is over the lowest two LLs. A LL consists of all n, m that satisfy LL index $\lambda = n + \frac{1}{2}(|m| + m) = \text{constant}$ (i.e. 0 or 1 for our specific case), and σ is the spin index (since at the magnetic fields considered here the Zeeman splitting is much smaller than the other relevant energy scales, we assume spin-degenerate states). Here, $\tilde{\omega}^2 \equiv \omega_0^2 + \omega_c^2$ with ω_0 the bare confining frequency and ω_c the cyclotron frequency. C_{ij} are the capacitance matrix elements (off-diagonal elements are always negative [17,22]), $D \equiv C_{00}C_{11} - C_{01}^2$. Here V_{gl} is defined relative to the gate voltage that induces $N_{0(1)}^0$ electrons (i.e. $N_{0(1)}^0$ is the number of electrons in LL0(1) at $V_{gl}=0$).

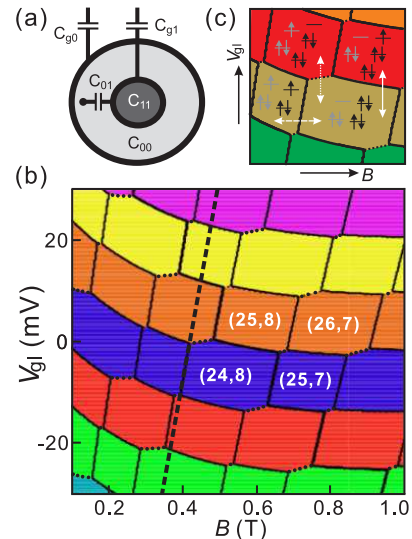


FIG. 2. (a) Schematic of the dot in terms of two Landau levels (LLs). (b) Results of numerical minimization of Eq. 1. Color stripes are regions of constant $N = N_0 + N_1$. Numbers in parentheses show N_0, N_1 . Black lines bound regions of constant N_0 . Dotted lines show “ N_1 boundaries”. The N_1 boundary lengths alternate (compare to Fig. 1b). Capacitances and dot parabolicity estimated for $N_0^0 = 25$, $N_1^0 = 10$, $B_0 = 0.6$ T: $C_{00} = 3.3$, $C_{11} = 2.2$, $C_{01} = -2.1$, $C_{g0} = -0.10$ and $C_{g1} = -0.056$ (all in aF), $\omega_0 = 0.4$ meV. The dashed line is the approximate 3rd LL filling boundary. (c) Schematic honeycomb structure in the B, V_{gl} plane resulting from the double dot model. Typical occupancy configurations (energy vs. position) of LL1 (gray arrows) and LL0 (black arrows) at the dot boundary are shown for different honeycomb cells.

First, we estimate capacitances C_{ij} and bare confining potential ω_0 from the full SDF calculations for (N_0^0, N_1^0) electrons and for a “central” magnetic field B_0 (see caption, Fig. 2) [23]. Then, we numerically minimize Eq. 1 with respect to N_0 and N_1 , keeping C_{ij} and ω_0 constant (even though in principle these change slightly over our (B, V_{gl}) range). We find a “honeycomb” structure characteristic for DDs [17]. As shown in Figs. 2b and c, this structure clearly emerges and compares reasonably well with the experimental data of Fig. 1b.

Figure 2c schematically shows the population of the lowest two LLs in four neighboring honeycomb cells. B principally induces depopulation of LL1 to LL0; V_{gl} changes the total electron number $N = N_0 + N_1$. Note that the dotted boundaries between N_1 and $N_1 + 1$ (“ N_1 borders”), are considerably shorter than the solid boundaries between N_0 and $N_0 + 1$. Weak *tunnel* coupling of the inner LL (LL1) to the leads causes these N_1 borders to appear as gaps (or small offsets) in the Coulomb oscillations [24], which are clearly seen in Fig. 1b. Analysis of Eq. 1 shows that the length of the N_1 borders, in both B and V_{gl} , is proportional to $C_{11} - |C_{01}|$. Therefore, the short N_1 borders indicate that LL0 strongly screens (via C_{01}) the inner LL1. In other words, most of the self-capacitance of LL1 is taken up by capacitance to LL0. This screening of the inner LL is ultimately what produces the chessboard pattern of the Kondo conductance (see below). Furthermore, the length of the N_1 borders in Figs. 2b,c alternates, as observed in the experimental data (Fig. 1b). The shorter N_1 borders appear as only small discontinuities in the experimental Coulomb oscillations. From Eq. 1 it follows that this alternating pattern results from the spin degeneracy of the FD levels. Specifically, increasing B and transferring a LL1 electron to LL0, at fixed N , costs an additional, LL0 level spacing when N_0 changes from even to odd. The main feature of the experimental data that is not present in Figs. 2b,c is the increased valley conductance due to the Kondo effect. We show below, using our SDF analysis, that this increased valley conductance appears in the hexagons where N_0 is odd.

Our SDF calculations for realistic, 3D, lateral semiconductor quantum dot structures have been thoroughly described before [25]. We compute self-consistent eigenvalues $\varepsilon_{p\sigma}$, eigenfunctions $\psi_{p\sigma}$, occupancies $n_{p\sigma}$ and tunneling coefficients $\gamma_{p\sigma}$, with p the orbital and σ the spin indices, as well as the total interacting energy F of the dot-gate-leads system, all as a function of N , V_{gl} and B . However, we cannot compute the coherent Kondo-assisted conductance of the dot from the ground state properties provided by the SDF calculation. Instead, we introduce an effective Kondo parameter, which enables us to reproduce the conductance modulation characteristic for the chessboard pattern.

In Ref. [12] it was qualitatively argued that the alternating Kondo conductance with varying B at fixed N

observed in their experiments in the strong edge state regime resulted from Coulomb regulated redistribution of electrons, one at a time, from LL1 to LL0. Since LL0 was assumed much more strongly coupled to the leads, the Kondo effect was argued to occur only when N_0 is odd. Here, the computed electronic structure allows us to *quantitatively* exhibit this depopulation process, to show how it varies in phase from one Coulomb valley to the next and to show how the B -dependent tunneling coefficients affect the structure of individual chessboard fields. The model’s assumption of spin-degenerate states is accounted for at the end of the paper.

In the standard derivation of the s-d model from the Anderson model [26], a Schrieffer-Wolff transformation is used to define an effective coupling between spin-degenerate states of the dot (or impurity) via virtual electron exchange with a neighboring Fermi sea. These co-tunneling processes then lead to coherent hybridization of the degenerate states, which results in a logarithmic increase of the conductance at low temperature, a feature of the Kondo effect in quantum dots. In general, a dot can contain many singly occupied electron states, for which spin-flip can occur via co-tunneling contributing to the Kondo coupling. In order to estimate the contribution of all singly-occupied states to the Kondo effect, we define a parameter K , which we call Kondo parameter, as the sum of all co-tunneling amplitudes that leave the ground state of the system unchanged except for the flip of a single spin

$$K \equiv \sum_{p,\sigma} n_{p,\sigma} (1 - n_{p,\bar{\sigma}}) \sqrt{\gamma_{p,\sigma} \gamma_{p,\bar{\sigma}}} \left[\frac{1}{F(N+1, V_{gl}, B) - F(N, V_{gl}, B)} + \frac{1}{F(N-1, V_{gl}, B) - F(N, V_{gl}, B)} \right] \quad (2)$$

where $\bar{\sigma}$ is the spin opposite to σ . We conclude from the experimental data that the spin polarization of the leads is negligible, in contrast to Ref. [24].

A color scale plot of K in the (B, V_{gl}) plane is shown in Fig. 3, for $N = 32$ to 39. Here, the V_{gl} dependence has been approximated as follows. The two denominators in Eq. 2 are additions energies, which are, to a good approximation, linear in V_{gl} and vanish at the Coulomb oscillations. Thus, $F(N+1, V_{gl}, B) - F(N, V_{gl}, B) \approx (e^2/2C) + e\alpha(V_{gl} - V_{gl}^{N, \min}) + \varepsilon_{N+1}$, where $(e^2/2C) \equiv (\partial^2 F / \partial N^2)$ defines C , and $\partial F(N, V_{gl}^{N, \min}, B) / \partial N = 0$ defines the valley center gate voltage, $V_{gl}^{N, \min}$, and where $\alpha = C_{dot-gate} / C$ is the lever arm (a similar analysis holds for the second energy denominator). By calculating the full electronic structure only near the valley centers, we can determine the CI parameters $V_{gl}^{N, \min}$, C and α and thereby show the V_{gl} dependence of K due to the

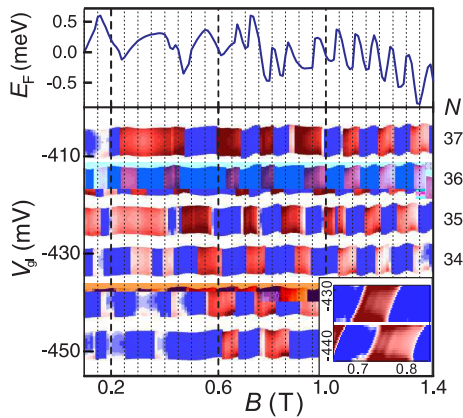


FIG. 3. Color scale plot of Kondo parameter K in the B, V_{gl} plane. Red (blue) corresponds to large (small) K . Third LL filling begins below $\sim 0.5T$. K is calculated in the Coulomb valley center at each B (see text). Upper panel shows Fermi energy vs. B for $N = 37$ and fixed $V_{gl} = -407$ mV. E_F drops at each reconstruction (i.e. at the end of each Kondo zone). Inset, K fully calculated from Eq. 2 on fine mesh for small B, V_{gl} region (i.e. no approximation for the V_{gl} dependence is used here).

addition energies, Fig. 3. The full calculation of Eq. 2 on a mesh of B, V_{gl} values, which is numerically taxing, is shown for a small region in the inset to Fig. 3.

The alternating pattern of Kondo “zones” in successive Coulomb valleys is evident. Even in this low magnetic field regime, the coupling of the LL0 states to the leads typically exceeds that of the LL1 states by two orders of magnitude. Therefore, although the parameter K is a sum of all possible co-tunneling amplitudes, the amplitudes of the LL0 states dominate. Hence, even when N is odd, K is negligible as long as N_0 is even.

Within a Kondo zone an abrupt increase of K is followed by a gradual decrease. This results from the contraction, with B , of the half-filled orbit at the dot edge, and the resulting decrease of its tunnel coefficient. When another electron depopulates from LL1 to that orbit, that spin flip process is no longer available, and K collapses. Depopulation of LL1 coincides with a drop of the dot’s Fermi level [28] relative to the leads (Fig. 3, top panel). The denominators in Eq. 2 are responsible for the increase of K away from the valley centers; a feature which is clearly observed in the experiment Fig. 1b.

The approximation used in Fig. 3 includes the V_{gl} dependence of the charging energies, but not that of the $n_{p,\sigma}$. The latter dependence, specifically that of the transfer from LL1 to LL0, controls the slant of the chessboard fields. This slant only emerges in the calculation of K without approximation, as shown for a small region of V_{gl} and B in the inset to Fig. 3.

Finally, we comment on our assumption of spin-degenerate states. For N odd, this only requires that the Zeeman splitting ($\sim 10 \mu\text{eV}$) is negligible, which is the case in the B range considered. However, for N even, a

singly filled orbital in LL0 implies another one in LL1 and these electrons have, in general, an exchange interaction. In Ref. [27] it was found that this exchange interaction diminishes rapidly with N . For our dot, we explicitly determine the singlet-triplet splitting for various (even) N and B by computing separate ground states constrained to $S = 0$ and $S = 1$. We find that the splitting is typically tens of μeV . The experimental signature of a split ground state is a split Kondo resonance (in source-drain voltage). Our analysis suggests that this splitting, which has been observed [9,15], would be characteristic of N even in regimes where Zeeman energy is small.

We acknowledge financial support from the DARPA grant number DAAD19-01-1-0659 of the QuIST program.

-
- [1] L.P. Kouwenhoven *et al.*, Electron transport in quantum dots, in Mesoscopic Electron Transport, edited by L.L. Sohn *et al.*, (Kluwer, Series E **345**, 1997), p.105-214.
 - [2] L.I. Glazman and M.E. Raikh, JETP Lett. **47**, 452 (1988).
 - [3] T.K. Ng and P.A. Lee, Phys. Rev. Lett. **61**, 1768 (1988).
 - [4] D. Goldhaber-Gordon *et al.*, Nature **391**, 156 (1998).
 - [5] S.M. Cronenwett *et al.*, Science **281**, 540 (1998).
 - [6] J. Schmid *et al.*, Physica B **256-258**, 182 (1998).
 - [7] S.M. Maurer *et al.*, Phys. Rev. Lett. **83**, 1403 (1999).
 - [8] W.G. van der Wiel *et al.*, Science **289**, 2105 (2000).
 - [9] S. Sasaki *et al.*, Nature **405**, 764 (2000).
 - [10] J. Nygård *et al.*, Nature **408**, 342 (2000).
 - [11] J. Schmid *et al.*, Phys. Rev. Lett. **84**, 5824 (2000).
 - [12] M. Keller *et al.*, Phys. Rev. B **64**, 033302 (2001).
 - [13] W.G. van der Wiel *et al.*, Phys. Rev. Lett. **88**, 126803 (2002).
 - [14] D. Sprinzak *et al.*, Phys. Rev. Lett. **88**, 176805 (2002).
 - [15] C. Fühner *et al.*, Phys. Rev. B **66**, 161305(R) (2002).
 - [16] U.F. Keyser *et al.*, cond-mat/0206262 (2002).
 - [17] W.G. van der Wiel *et al.*, Rev. Mod. Phys. **75**(1), 1 (2003).
 - [18] P.L. McEuen *et al.*, Phys. Rev. B **45**, 11419 (1992).
 - [19] J.M. Kinaret and N.S. Wingreen, Phys. Rev. B **48**, 11113 (1993).
 - [20] N.C. van der Vaart *et al.*, Phys. Rev. Lett. **73**, 320 (1994).
 - [21] V. Fock, Z. Phys. **47**, 446 (1928); C.G. Darwin, Proc. Cambridge Philos. Soc. **27**, 86 (1930).
 - [22] M. Stopa, Y. Aoyagi and T. Sugano, Phys. Rev. B **51**, 5494 (1995).
 - [23] A small upward adjustment to the capacitances, by $< 50\%$, is then made which appears to reproduce the experimental data more faithfully. This might be attributed to stronger lead-dot capacitance in the experimental structure than that which is calculated.
 - [24] M. Ciorga *et al.*, Phys. Rev. Lett. **88**, 256804 (2002).
 - [25] M. Stopa, Phys. Rev. B **54**, 13767 (1996); M. Stopa, Semicond. Sci. Technol. **13**, A55 (1998); M. Stopa, Physica E **10**, 103 (2001).
 - [26] A.C. Hewson, *The Kondo Problem to Heavy Fermions* (Cambridge, Cambridge, England, 1993).
 - [27] S. Tarucha *et al.*, Phys. Rev. Lett. **84**, 2485 (2000).
 - [28] E_F is defined by $N = \sum_i f[(\varepsilon_i - E_F)/k_B T]$, with ε_i Kohn-Sham levels, N fixed and f the Fermi function.